Tracking Electrons Produced by Compton Scatter within a Prompt Gamma Imaging Device

S W Peterson[1], M Hillebrand[1], D Mackin[2], E Draeger[3], S Beddar[2], J Polf[3]

[1] Department of Physics, University of Cape Town, Rondebosch 7700, South Africa
[2] Department of Radiation Physics, University of Texas MD Anderson Cancer Center, 1515 Holcombe Blvd, Houston, TX, USA
[3] Department of Radiation Oncology, University of Maryland School of Medicine, 22 South Greene St, Baltimore, MD, USA

Email: steve.peterson@uct.ac.za

Abstract. Proton therapy requires precise delivery of the accelerated particles to the cancerous tissue in order to maximize its considerable benefits. Unfortunately, there is no way to directly monitor the actual dose delivered to the patient. Prompt Gamma Imaging (PGI), specifically using a Compton camera, is a promising option for in vivo verification of the 3D dose distribution. A Compton camera relies on an incident gamma undergoing multiple Compton scatters within its multiple stages. The information (energy deposited and location) from the Compton scatters (2 or more) can be used to reconstruct a cone of origin. With a sufficient number of cones and appropriate image reconstruction techniques, a 3D image of the dose can be produced. Of course, the accuracy of the image reconstruction relies heavily on the quality of the data measured by the detector, specifically the energy and position of the detected electron. This work uses the Geant4 Monte Carlo toolkit to track the Compton electrons within the individual stages of the Compton camera in order to better understand the accuracy of the detected electron position and energy. The energy and range of the secondary electrons are broken down by scatter sequence order. Two detector configurations were investigated. The work provided some clear indications of the expected accuracy from the energy and position measurements of the electrons in a Compton camera.

1. Introduction

Proton therapy was first performed in South Africa more than 20 years ago at iThemba LABS in Somerset West. In the last 5-10 years, there has been a huge increase in the number of clinical proton therapy treatment facilities around the world due primarily to the decreasing cost of particle accelerators. Since the 1940s, the benefits of protons for the treatment of cancer have been well known. The basic advantage of proton radiation therapy is the way that protons interact with material, specifically a minimal entrance dose and a sharp increase in energy deposition near the end of the proton range. The lack of exiting protons has made it difficult to produce an actual image of the dose deposition within the patient; and the uncertainty in the dose delivery has made the need for an in-vivo dose verification system extremely important. A suggested method of dose verification is the use of the secondary gammas produced by proton-nucleus inelastic collisions in the patient [1]. These "prompt" gammas are produced during treatment at the location where the dose is deposited, making them an ideal candidate [2].

There are a number of ways to detect these prompt gammas, using both physically and electronically collimated devices [3-6], but this work concentrates on a device called a Compton camera. A Compton camera, originally developed for use in astronomy applications [7], relies on a particular gamma ray to interact two or more times within the detector, capturing energy and position data each time. This data can then be used to project the expected gamma creation position onto a cone. As more prompt gammas are detected, the intersection of the cones can be used to reproduce an image of the dose deposited within the patient. The advantage of this type of device would be a relatively compact system that could produce full three-dimensional pictures of the dose being deposited in the patient [8].

Several groups are working on developing a Compton camera for prompt gamma detection [4, 9-12], but this work will focus on understanding an existing solid-state system consisting of multiple detection stages composed of Cadmium zinc telluride, (CdZnTe) or CZT [13]. The reconstruction of useable images from a Compton camera relies heavily on the information (energy deposited and location) gathered from each Compton interaction. Any uncertainty in this data will result in difficulties in image reconstruction and consequently, reduced image quality. A primary source of position uncertainty has to do with the recorded position of electron produced during the Compton interaction.

This work uses the Geant4 Monte Carlo toolkit to track the Compton electrons within the individual stages of the Compton camera in order to better understand the accuracy of the detected election position and energy. The energy and range of the secondary electrons are broken down by scatter sequence order while two different detector configurations were investigated. These results are used to make some estimation of the expected deviations in the energy and position measurements due to the electrons in the Compton camera.

2. Method

2.1. Compton Camera

2.1.1. *Basics.* The basic function of a Compton camera (CC) is to track an incident gamma as it undergoes multiple Compton scatters, recording the energy deposited (ΔE) and the position of each of the Compton interactions. There are two basic types of events, a double-scatter event where the gamma scatters once and is then absorbed, or a triple-scatter event where the gamma has two Compton interactions followed by a third position-recording event (Compton, photoelectric, or pair production). For double-scatter events, the initial energy (E_0) of the gamma is simply determined by

$$E_0 = \Delta E_1 + \Delta E_2, \tag{1}$$

where ΔE_1 and ΔE_2 is the energy deposited during the Compton and photoelectric interactions. For triple-scatter events, the initial energy is found using [14]

$$E_0 = \Delta E_1 + \frac{1}{2}\left(\Delta E_2 + \sqrt{\Delta E_2^2 + \frac{4\Delta E_2 m_e c^2}{1-\cos\theta_2}}\right), \tag{2}$$

where θ_2 is the scattering angle of the second interaction, m_e is the mass of the electron and c is the speed of light. The scattering angle is determined by the positions (p_1, p_2, p_3) of the three interactions (see figure 1). The initial scattering angle (θ_1) can be determined by

$$\cos\theta_1 = 1 + m_e c^2\left(\frac{1}{E_0} + \frac{1}{E_0 - \Delta E_1}\right). \tag{3}$$

The origin position of the gamma cannot be determine explicitly, but is restricted to the surface of the "cone-of-origin", which has an opening angle θ_1 and apex p_1. The axis of the cone is along the line containing the points p_1 and p_2. This cone (along with many others) can then be used to produce an image of the original gamma distribution using an image reconstruction technique.

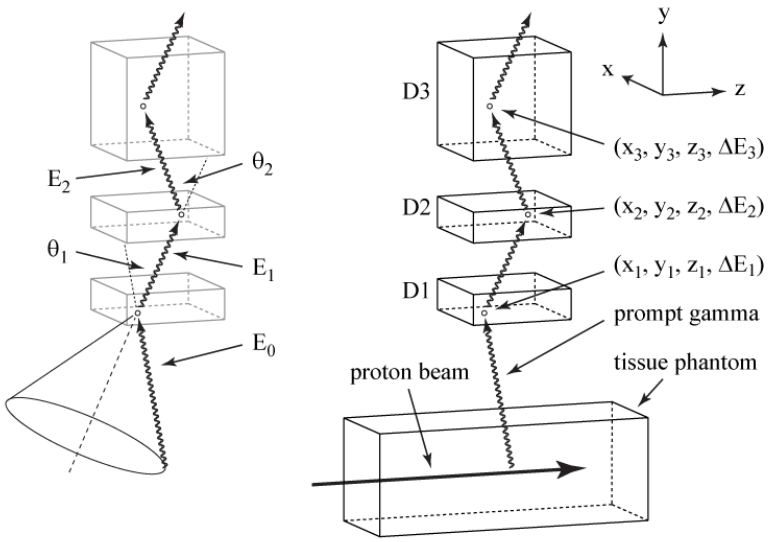

Figure 1. Diagram of the 3-stage Compton camera setup in parallel-plane geometry showing the Compton scatter angles (θ_1, θ_2) and the gamma ray energy (E_0, E_1, E_2) as it travels through the detectors (D1, D2, D3), as well as the projected code used to reconstruct the images. Figure reproduced from ref 4.

2.1.2. *Compton Electrons.* There are number of uncertainties that can hinder the effectiveness of a Compton camera, such as Doppler broadening and finite energy and spatial resolutions of the CC detectors. This work will look specifically at the impact of the recoil electron on the two measured quantities: deposited energy (ΔE) and interaction position (p). We are able to focus solely on the recoil electron by removing Doppler broadening from our simulations and using an "ideal" detector with infinite position and energy resolution.

2.1.3. *Detector Configuration.* Two different detectors were used for the work. First, the actual detector, the Polaris J detection system from H3D [15, 16] was used to determine the impact of the Compton electron in a realistic situation. Second, an "infinite" detector was used to explore specific features of the Compton electron.

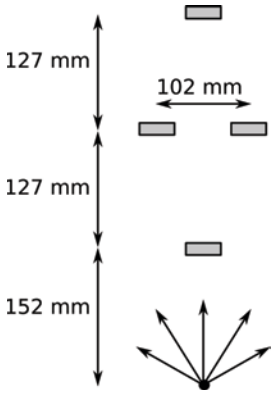

Figure 2. Configuration of the experimental Polaris J setup.

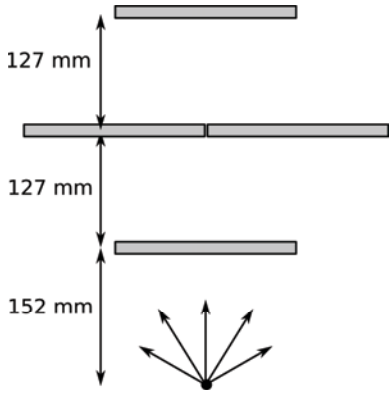

Figure 3. Configuration of the simulated "infinite" detector.

The Polaris J system [13] consists of four stages, each stage containing four CZT crystals, with two stages having 20 mm x 20 mm x 15 mm detector crystals, while the other two have 20 mm x 20 mm x 10 mm crystals. For this work, the four stages were arranged in a 1-2-1 configuration (as shown in figure 2) with a spacing of 5 inches (127 mm, center to center) between the three layers of detectors. The two middle detectors were each offset 2 inches (50.8 mm) from the CC axis, while the front and back detectors were placed in line with the CC axis. The CC was positioned 6 inches (152.4 mm) from the source. This configuration mimics the standard experimental setup used in previous work [13].

The infinite detector was composed of four 200 mm x 200 mm stages with the thickness varying from 5 to 25 mm. Each stage was simulated as a single CZT crystal and the four stages were arranged in a 1-2-1 configuration (as shown in figure 3) to mimic the Polaris J setup described above. This configuration was used in order to explore the Compton electron while saving computation time.

2.2. Monte Carlo

The simulations performed for this work used a previously developed Geant4 (v9.4.p01) model used for CC efficiency studies [4, 17], an image reconstruction study [8] and experimental comparisons [13]. The model has been expanded to look specifically at Compton electrons, but uses the same settings as previous work [4, 8, 13, 17]. An isotropic point source of 4.44 MeV gammas was used to produce the Compton scatters. The 4.44 MeV source was used to replicate one of the primary prompt gammas produced during proton irradiation. Only electrons produced during a triple-scatter event were tracked. An electron range cut of 0.01 mm was used (equivalent to an energy threshold of 44.4 keV) and each run started with 1 x 10^8 gammas. Escaped electrons were not tracked after they left the detector, although any energy deposited within a detector and the range of the electron was recorded. The electron energy deposition was recorded by scatter and also compared to the energy lost by the gammas. The Polaris J simulation required 1.1 x 10^{11} gammas.

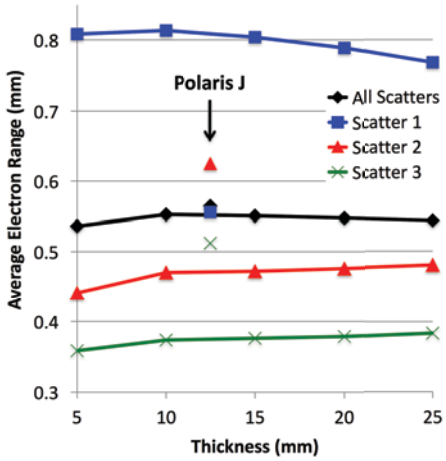

Figure 4. Average electron range for infinite detector at various thicknesses, with a breakdown by individual scatters. Average values for the Polaris J detector also included.

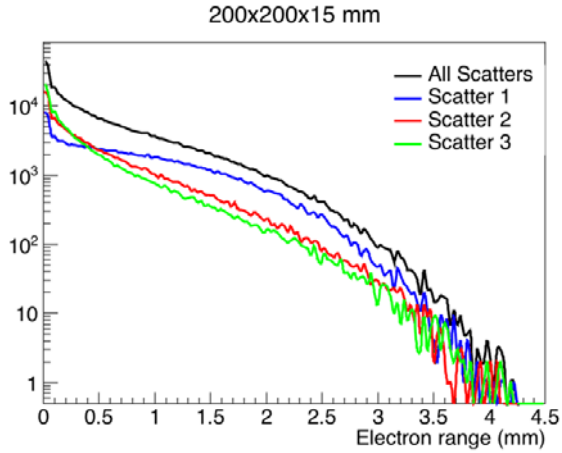

Figure 5. Histogram of the electron range broken down by scatter for the infinite detector with a 15 mm thickness. The y-axis (log scale) is the number of gammas at a given range.

3. Results and Discussion

3.1. Electron Range

Figure 4 shows the average electron range for the infinite detector at various thicknesses. The range of the electron for the first Compton interaction (Scatter 1) is significantly longer than for the other interactions, due to the higher incident gamma energy. The scatter angle of the Compton interaction will also impact the electron energy and range, but due to the geometry of the infinite detectors, the range of scatter angles for each scatter remains approximately the same, and thus will only have a smaller contribution on the electron range than the incident gamma energy. There is also a slight decrease in the range of the first scatter as thickness increases due to the fact that as thickness increases, the number of escaping electrons decreases (see Figure 6). Figure 5 shows the distribution of electron ranges for the 15 mm thick infinite detector. The first scatter consists primarily of electrons with long ranges in comparison to the second and third scatters. Figure 6 shows the sharp decrease in the number of escaping electrons with increasing thickness.

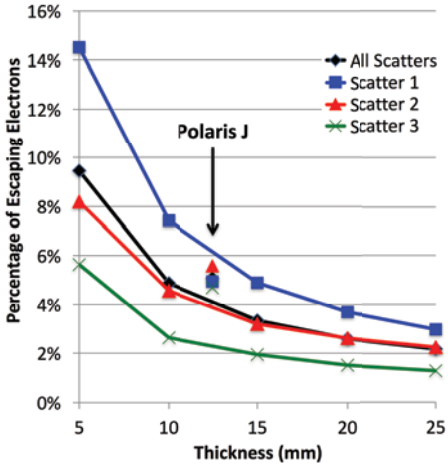

Figure 6. Percentage of Compton electrons that escape from the infinite detector broken down by scatter. Results from the Polaris J detector are also shown.

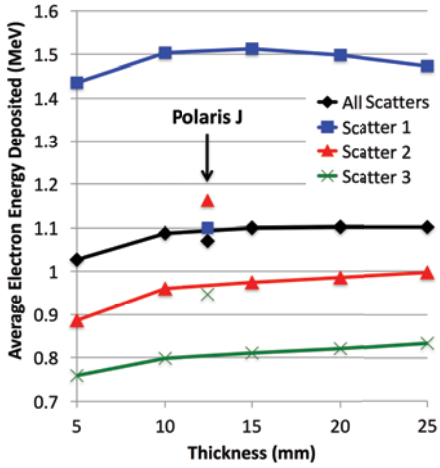

Figure 7. Average electron energy deposited in the infinite detector at various thicknesses, including the breakdown by individual scatters. Results from the Polaris J detector also shown.

3.2. Electron Energy Deposition

Figure 7 shows the average energy deposited by the electron in the infinite detector. Again, the first scatter has a much larger energy deposition and starts to decrease at the largest thicknesses due to the smaller number of escaping electrons while the second and third scatters are capturing more energy. Figure 8 shows the distribution of energy deposition for the 15 mm thick infinite detector (top panes). The top left shows the energy lost by the Compton gammas while the top right shows the energy deposited by the Compton electron. Notice a slight left-hand shift in the electron energy curve indicating a net loss of energy deposition, particularly at the high energies. For the 15 mm thick infinite detector, the average electron deposition for all scatters is 0.2 MeV below the expected value (energy lost by the Compton gammas).

3.3. Polaris J

Figures 4, 6, 7 show results from the simulated Polaris J Compton camera detector overlaid on the infinite detector results. In each figure, the Polaris J results show less deviation between the different scatter interactions while the overall values line up quite closely. In contrast to the infinite detector, the second scatter in the Polaris J detector produces the longest range (Figure 4) and the largest energy deposition (Figure 7) instead of the first scatter. The reason for this can be seen in Figure 8 (bottom panes). Notice the large bump in the energy deposition of the second scatters around 1.5 MeV, resulting in a higher average energy deposition and consequently, a higher average range. Because of the Polaris J detector geometry, a successful triple scatter interaction will have a very narrow angular window and due to the angular dependence of the Compton equation, will, consequently, have a very narrow energy acceptance window, resulting in the 1.5 MeV energy bump.

3.4. Deviations in Polaris J Measurements Due to the Compton Electron

The deviation in measured position by the Polaris J detector due to the path of the Compton electron is estimated to be 0.3 mm, which is roughly half of the simulated electron range, based on results from Figure 4. This assumption is likely an overestimation due to the fact that an electron path is not linear and does not take into account how the detector electronics capture the position of the interaction.

The deviation in measured energy deposition is estimated to be 0.2 MeV, which is the average energy difference between the expected energy lost by the gamma and the actual electron energy deposited.

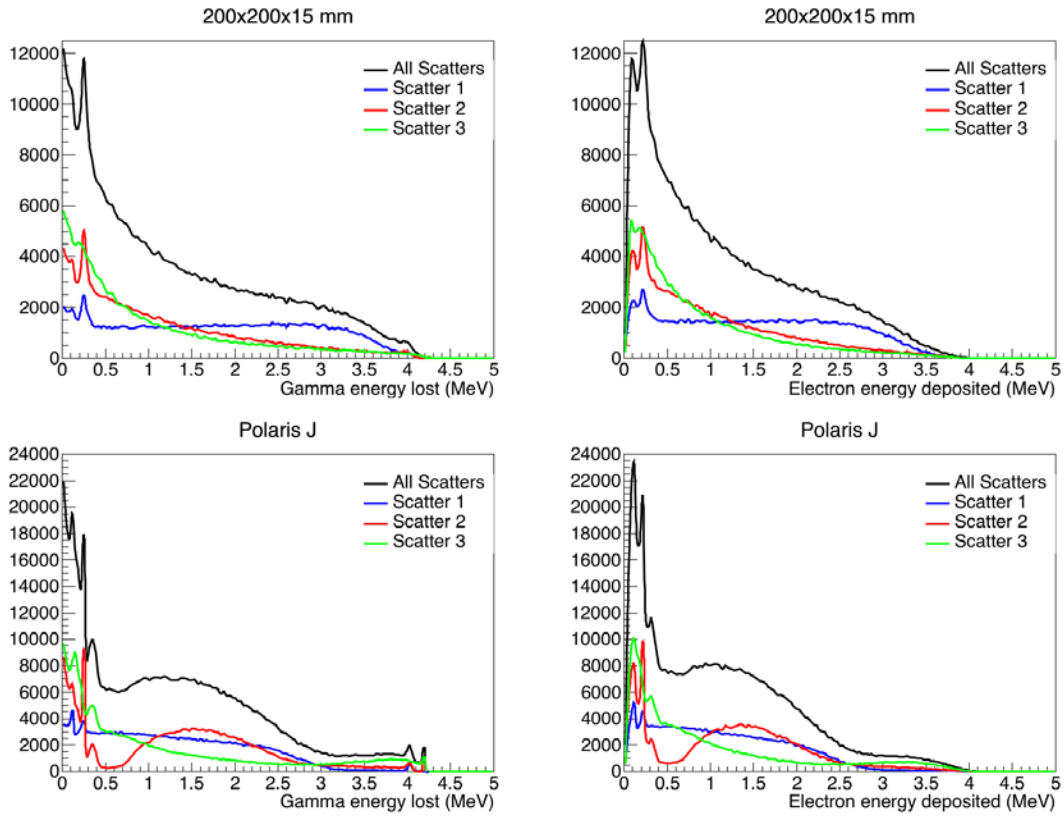

Figure 8. Histogram of the energy lost by the gamma (left panes) and the energy deposited by the electrons (right panes) for the 15 mm thick infinite detector (top panes) and the simulated Polaris J detector (bottom panes). The energy histograms are also broken down by scatter sequence number. The values on the y-axes are the number of gammas.

4. Conclusion

The Geant4-based Compton electron simulation estimated the deviations in the Polaris J detector to be 0.3 mm in position and 0.2 MeV in energy deposition for a 4.44 MeV gamma. The Compton electrons will certainly have an impact on a system that has stated resolutions of 1-2 mm and less than 0.1 MeV.

References

[1] Min C, Kim C H, Youn M and Kim J 2006 Appl. Phys. Lett. 89 183517
[2] Polf J C, Peterson S W, Ciangaru G, Gillin M and Beddar S 2009 Phys. Med. Biol. 54 731
[3] Polf J, Peterson S W, et al. 2009 Phys. Med. Biol. 54, N519
[4] Peterson S W, Robertson D and Polf J C 2010 Phys. Med. Biol. 55 6841
[5] Verburg J M, Riley K, Bortfeld T and Seco J 2013 Phys. Med. Biol. 58 L37
[6] Smeets J, et al. 2012 Phys. Med. Biol. 57 3371
[7] Deleplanque M A, et al. 1999 Nucl. Instrum. Methods Phys. Res. A 430 292
[8] Mackin D, Peterson S W, Beddar S, and Polf J 2012 Phys. Med. Biol. 57, 3537
[9] Richard M, et al. 2012 IEEE Trans. on Nucl. Sci. 59, 1850
[10] Seo H, et al. 2010 Nucl. Instrum. Methods Phys. Res. A 615 333
[11] Kurusawa S, et, al. 2012 Curr. App. Phys. 12 364
[12] Hueso-González F, et al. 2014 JINST 9 P05002
[13] McCleskey M, et al. 2015 Nucl. Instr. and Meth. Phys. Res. A 785 163
[14] Kroeger R, Johnson W, Kurfess J, Phlips B, and Wulf E 2002 IEEE Trans. Nucl. Sci. 49 1887
[15] He Z, et al. 1999 Nucl. Instrum. Methods Phys. Res. A 422 173
[16] Zhang F, He Z and Seifert C E 2007 IEEE Trans. Nucl. Sci. NS-54 843
[17] Robertson D, Polf J C, Peterson S W, Gillin M T, and Beddar S 2011 Phys. Med. Biol. 56 3047